DOI: https://doi.org/10.24425/amm.2025.154489

YANCHAO BAI<sup>©</sup><sup>1,2</sup>, WEIBIN WANG<sup>©</sup><sup>1,2</sup>, WEI WANG<sup>©</sup><sup>1,2\*</sup>

# THE EFFECT OF Cr AND V ON THE OXIDATION CHARACTERISTICS OF Fe-V ALLOY FROM VANADIUM SLAG AT HIGH TEMPERATURE

The influence of V and Cr on the weight gain due to oxidation of Fe-V alloy from vanadium slag at  $800^{\circ}$ C was studied. X-ray diffraction (XRD), scanning electron microscopy coupled to an energy dispersive spectrometer (SEM-EDS) and thermal gravimetric analysis (TGA) were employed to observe and analyze the oxidation products and surface morphology of Fe-V alloys. The results indicate that the oxidation kinetics curve of the Fe-V alloy, after undergoing 180 minutes of oxidation at  $800^{\circ}$ C, follows a linear trend. Moreover, the oxidation process is determined by the reaction rate of oxide formation. The oxidation products are Fe<sub>2</sub>O<sub>3</sub>, (Fe<sub>0.6</sub>Cr<sub>0.4</sub>)<sub>2</sub>O<sub>3</sub>, and CrVO<sub>4</sub>. The thickness of the oxide layer gradually increases with an increase in the V content. The oxide layer thickness of Fe-11V is the largest, approximately three times that of Fe-7V. Both the porous oxide layer structure and microcracks on the surface of the oxidation products play an important role in the sustained oxidation of Fe-V alloy. This work is useful for understanding the oxidation resistance of the alloy at high temperature.

Keywords: Fe-V alloy; vanadium; high-temperature oxidation; gain in weight; microstructure

### 1. Introduction

Recently, vanadium and its alloys have been paid more attention due to their superior physical and chemical properties, such as high melting point, high-temperature strength, favorable plasticity, and ductility [1-3]. These vanadium alloys are widely used in railways, bridges, aerospace, machine building, and other fields. However, vanadium metal has a strong affinity for oxygen. Oxygen environment has a solubility of up to 3.5% (atomic fraction) in vanadium metal in room temperature [4]. Therefore, O can permeate into the vanadium alloy matrix to form oxides distributed along grain boundaries during service, which has no protective effect on the matrix material, resulting in materials deterioration of the alloy [5]. In addition, the low melting oxides in V-alloys can also bring some harmful influences to the high-temperature performance [6-7].

With the pursuit of high heat resistance of materials in the field of engineering preparation, the research on high-temperature oxidation behavior of vanadium alloys has also developed rapidly. Kusumoto et al. [8] investigated the effect of vanadium on the high-temperature erosion-oxidation property of multicomponent iron-based alloys at 1173 K. It was confirmed that

the addition of V had a negative effect on the high-temperature oxidation resistance of the alloys owing to vanadium oxide attack. The evolution of coarse-grained σ-Fe<sub>48.1</sub>V<sub>51.9</sub> has been investigated by Costa et al under ball-milling in the steady supply of argon and air [9]. During the milling process, vanadium is oxidized preferentially to form V<sub>2</sub>O<sub>3</sub> with a nanostructure. With the extension of milling time (after about 140 h), Fe-V alloys with bcc and fcc structures begin to form a ternary Fe-V-O spinel phase. Ye et al. [10] reported that the oxidation products and morphologies of pure vanadium are diverse in the range of 300-600°C. With the increasing of temperature, the principal oxidation products of pure vanadium are transformed into  $VO_{0.03}$ ,  $VO_2$ , and  $V_2O_5$  in turn. When it is oxidized at 600°C, the oxidation products are distributed uniformly on the surface of the specimen in the form of fine-scale-shaped. Vanadium (V) and chromium (Cr) in vanadium-chromium (V-Cr) slag were separated successfully through heating V-Cr slag with Na<sub>2</sub>CO<sub>3</sub> [11]. In addition, the oxidation weight gain behavior of pure vanadium abides by parabolic law. So far, the oxidation behavior of various vanadium-containing alloy materials has been discussed in most of the studies. However, the published reports on the oxidation investigation of a solid Fe-V alloy at

Corresponding author: wwlyzwkj@126.com



HENAN UNIVERSITY OF SCIENCE AND TECHNOLOGY, COLLEGE OF MATERIALS SCIENCE AND ENGINEERING, LUOYANG 471023, CHINA

STATE KEY LABORATORY OF LIGHT SUPERALLOYS, LUOYANG, 471023, CHINA

high temperature are very limited. Numerous studies indicate that the complex oxidation behavior and oxidation products of vanadium alloy are subjected to the effects of multifarious factors such as oxidation temperature, oxygen partial pressure, alloy composition and so on [12-13].

This paper is developed on the basis of the foregone experiments of Fe-V alloy from vanadium slag and iron-rich red mud [14]. The aim of this work is to clarify the effect of the various V contents and chromium carbide on the oxidation behavior of Fe-V alloys in pure oxygen environment at 800°C. By means of kinetic analysis, XRD, SEM/EDS and TGA, the oxidation characteristics of Fe-V alloy at high temperature and the influence of V and Cr were discussed elaborately. This work can not only provide an in-depth investigation on the high-temperature oxidation behaviour and mechanisms but widen the engineering application of Fe-V alloy.

### 2. Materials and methods

### 2.1. Materials

Previously, Fe-V alloy has been prepared by carbothermal reduction method with iron-rich red mud and vanadium slag as raw materials [14]. The microstructure of the alloy was mainly composed of ferrite and pearlite. The chemical analysis of Fe-V alloy studied is listed in TABLE 1.

TABLE 1 Chemical composition of the tested samples

| Cample | Element content/wt.% |       |      |      |      |      |      |
|--------|----------------------|-------|------|------|------|------|------|
| Sample | Fe                   | V     | C    | Cr   | S    | Si   | Mn   |
| Fe-7V  | 83.37                | 6.91  | 4.19 | 3.11 | 0.08 | 0.60 | 1.74 |
| Fe-8V  | 83.03                | 8.12  | 3.64 | 2.99 | 0.09 | 0.52 | 1.61 |
| Fe-9V  | 82.47                | 9.37  | 3.58 | 2.63 | 0.08 | 0.49 | 1.38 |
| Fe-11V | 81.95                | 11.04 | 2.94 | 2.27 | 0.06 | 0.35 | 1.39 |

### 2.2. Oxidation experiment

Before the oxidation experiment, the surface of each sample was mechanically ground to 1200 grit size with emery papers, followed by ultrasonic cleaning in ethanol. The mass of each sample was weighed and recorded as the initial weight before oxidation. The oxidation experiment was performed in a vertical-type tube furnace, equipped with a high-precision balance connected to a computer. The corundum crucible with samples was hung from the recording balance by an Alloy 625 suspension wire into the uniform temperature zone of the vertical tube furnace. In each run, a sample was heated in an argon atmosphere at a heating rate of 8°C/min until it reached 800°C. Then, oxygen with a flow rate of 400 ml/min was introduced to the furnace for 180 min isothermal oxidation test. After the test, the samples were slowly cooled to 25°C in Ar environment to avoid re-oxidation and removed from the furnace. The weight

change of each sample was recorded by the balance and transmitted to the computer once every minute.

### 2.3. Measurement characterization

The oxidation products were analyzed and detected by the Bruker D8 Advance X-Ray Diffraction (XRD) with a scanning angle of 20°-80°. The morphology and chemical composition of the oxidized surface and cross-section of samples were observed and performed using a JSM-7800F field-emission-gun scanning electron microscope (FEG-SEM) equipped with energy dispersive spectrometer (EDS).

#### 3. Results and discussion

# 3.1. Oxidation kinetics curves of the tested samples at 800°C

Fig. 1 shows oxidation kinetics curves that reflect the change of oxidation weight gain per unit surface area of four samples exposed in O<sub>2</sub> with time at 800°C. Owing to the heterogeneity of the specimens, 2 various samples were taken to measure the mass change under the same conditions. The error on the total mass change is about 3.26%. As can be seen from Fig. 1, these curves obey linear law. This is consistent with previous reports [3]. Therefore, Eq. (1) was used to fit and analyze the kinetics data:

$$\Delta W = kt + C \tag{1}$$

where  $\Delta W$  is the mass gain per unit area in  $\mu g/mm^2$ , k is the parabolic oxidation rate constant in  $\mu g \cdot mm^{-2}min^{-1}$ , t is oxidation time in min, and C is the constant. The fitting results are listed in TABLE 2. The determinations coefficient  $R^2$  in TABLE 2 are all not lower than 0.85, indicating that the parabolic law is in good agreement with the oxidation kinetics curve of the samples.

Generally speaking, the oxidation of cast iron alloys mainly includes two aspects: the oxidation weight increase of the iron matrix and the oxidation decarburization weight loss caused by carbon combustion, and the former is always higher than the latter [15]. Therefore, the quality change of iron alloys during high-temperature oxidation is actually the sum of the weight increase caused by the growth of the oxide layer and the weight loss caused by carbon combustion. During the oxidation process, four kinds of samples exhibited significant oxygen absorption and weight gain behavior. Based on the comprehensive analysis of Fig. 1 and TABLE 2, it can be concluded that there is a linear relationship between the oxidation weight gain of the sample and the oxidation time, indicating that no protective oxide film has been formed on the surface of the sample during the oxidation process. The reaction rate of generating oxides has a close relationship with the oxidation process. At the same temperature, the oxidation weight change per unit area within the same oxidation time rises with the increase of V content. After

180 minutes of oxidation, the oxidation weight increase per unit area of the four samples is about  $38.619 \,\mu\text{g/mm}^2$ ,  $60.729 \,\mu\text{g/mm}^2$ ,  $74.262 \,\mu\text{g/mm}^2$ , and  $100.393 \,\mu\text{g/mm}^2$ , respectively. The oxidation weight gain of Fe-11V is the highest, and its antioxidant activity is the worst. Furthermore, the oxidation rate constant k in TABLE 2 shows a gradual increase. Obviously, the higher is the V content, the higher is the oxidation rate.

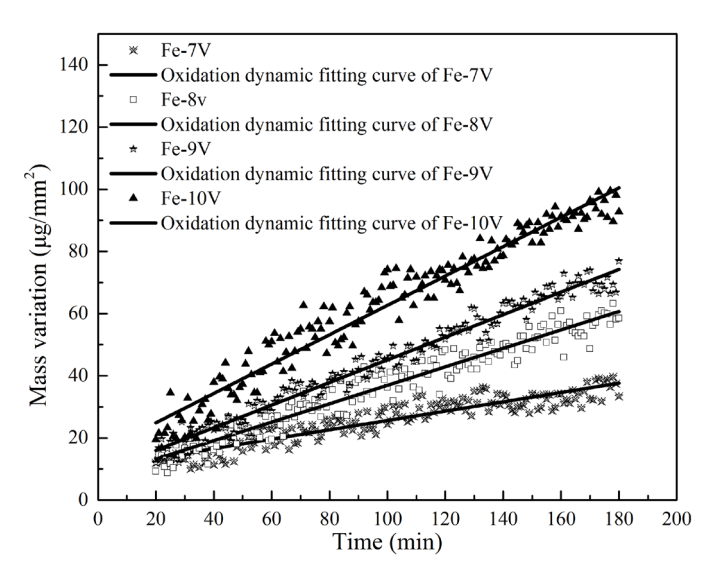


Fig. 1. Mass change of Fe-V alloy during oxidation at 800°C

TABLE 2 Fitting results of oxidation model

| Materials | $k/\mu g \cdot mm^{-2}min^{-1}$ | C     | $R^2$ |  |
|-----------|---------------------------------|-------|-------|--|
| Fe-7V     | 0.169                           | 8.199 | 0.882 |  |
| Fe-8V     | 0.297                           | 7.269 | 0.939 |  |
| Fe-9V     | 0.364                           | 8.742 | 0.971 |  |
| Fe-9V     | 0.364                           | 8.742 | 0.9   |  |

### 3.2. XRD analysis of oxide layer surface

Phase analysis of the outermost oxidation products of Fe-V alloys was performed by X-ray diffractometer. As indicated in Fig. 2, the outermost oxidation products of the samples after oxidation are mainly composed of Fe<sub>2</sub>O<sub>3</sub>, (Fe<sub>0.6</sub>Cr<sub>0.4</sub>)<sub>2</sub>O<sub>3</sub>, and CrVO<sub>4</sub>(a solid solution of Cr<sub>2</sub>O<sub>3</sub> and V<sub>2</sub>O<sub>5</sub>). According to the oxidation kinetics curve, it is apparent that none of these three oxidation products possess antioxidant properties and is unable to inhibit the occurrence of oxidation reactions. The diffraction peak intensity of oxidation products rises with an increase in V content, indicating a deepening degree of alloy oxidation. The primary metallic element in the alloy sample is Fe and as a result the predominant outermost oxidation product is Fe<sub>2</sub>O<sub>3</sub>. Compared with Fe and Cr, V is oxidized more easily, owing to their stronger affinity with O. Because of the lower mass fraction of Cr in samples, it is difficult to form a complete and protective Cr<sub>2</sub>O<sub>3</sub> layer during the initial oxidation stage. At high temperature, the Cr<sub>2</sub>O<sub>3</sub> crystal has a orthorhombic structure: lattice constant a = 3.55Å, b = 4.26 Å, c = 11.6 Å.  $V_2O_5$  also has a orthorhombic structure, which can dissolve in the orthorhombic  $Cr_2O_3$ . Therefore, there is a small amount of  $CrVO_4$ , but not individual  $V_2O_5$  crystal. In addition, Fe and Cr are infinitely miscible, and there is a similar atomic radii for Cr and V, resulting in the substitution of Cr atoms in chromium oxides by Fe and V, forming composite oxides (Fe<sub>0.6</sub>Cr<sub>0.4</sub>)<sub>2</sub>O<sub>3</sub> and CrVO<sub>4</sub>. This disrupts the continuity of chromium oxides with protective properties, leading to violent oxidation reactions. The occurrence of vanadium oxide in the oxide layer may be attributed to the complete oxidation of the low-valent vanadium oxide in the initial stage.  $V_2O_5$  with a melting point of round 670°C easily escapes from the oxide layer and evaporates into the furnace gas at the high temperature of 800°C [16].

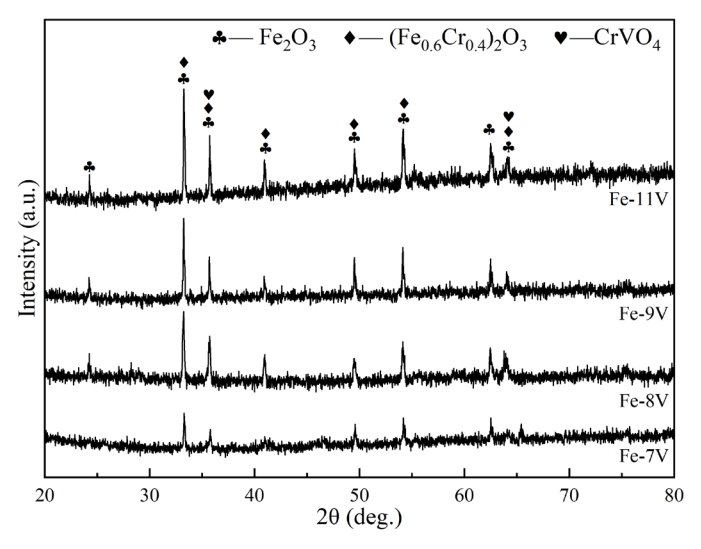


Fig. 2. The XRD diffraction of oxidation products of Fe-V alloys at 800°C

## 3.3. Surface morphologies of oxide layer

Fig. 3 indicates the surface morphologies of the Fe-V alloy after 180 minutes oxidation at 800°C. The figures reveal that the surfaces of all four Fe-V alloys are covered with a thick layer of oxidation products. For Fe-7V, the surface of the oxide layer appears relatively flat, predominantly consisting of irregular cone-shaped oxide products with well-separated particles and a relatively uniform size of approximately 2-4 µm. With the increase in V content, as indicated by the yellow arrow in Fig. 3(c), clusters of oxidation products begin to emerge on the surface of the previously flat oxide layer. The short tubular oxide particles within these clusters are slightly larger than that in the flat oxide layer, suggesting a gradual growth of the oxide particles and further deepening the oxidation level. For Fe-9V, the cluster with elongated oxidation products becomes larger on the surface of the oxide layer. In addition, there are small microcracks on these elongated oxides. Oxygen ions continuously diffuse and penetrate into the interface between the alloy and the oxide layer through these microcracks, promoting the oxidation reaction of the metal. The surface of the oxide layer on the Fe-11V sample exhibits severe cracking and detachment, with the oxidation

products primarily taking the form of elongated particles measuring 5-8 µm. The main reason is that the continuous oxidation reaction causes the original small-sized oxide particles to grow and squeeze each other, resulting in the generation of growth stress. As the oxide layer grows, the stress continuously increases. Once it surpasses a certain upper limit, the stress released ultimately results in the cracking and detachment of the oxide layer, providing additional pathways for the diffusion of oxygen ions into the matrix [17-18]. Therefore, the higher is the V content in the alloy, the greater is the number of pathways for oxygen ions to freely permeate the alloy matrix, leading to ongoing oxidation reactions and an increase in oxidation weight.

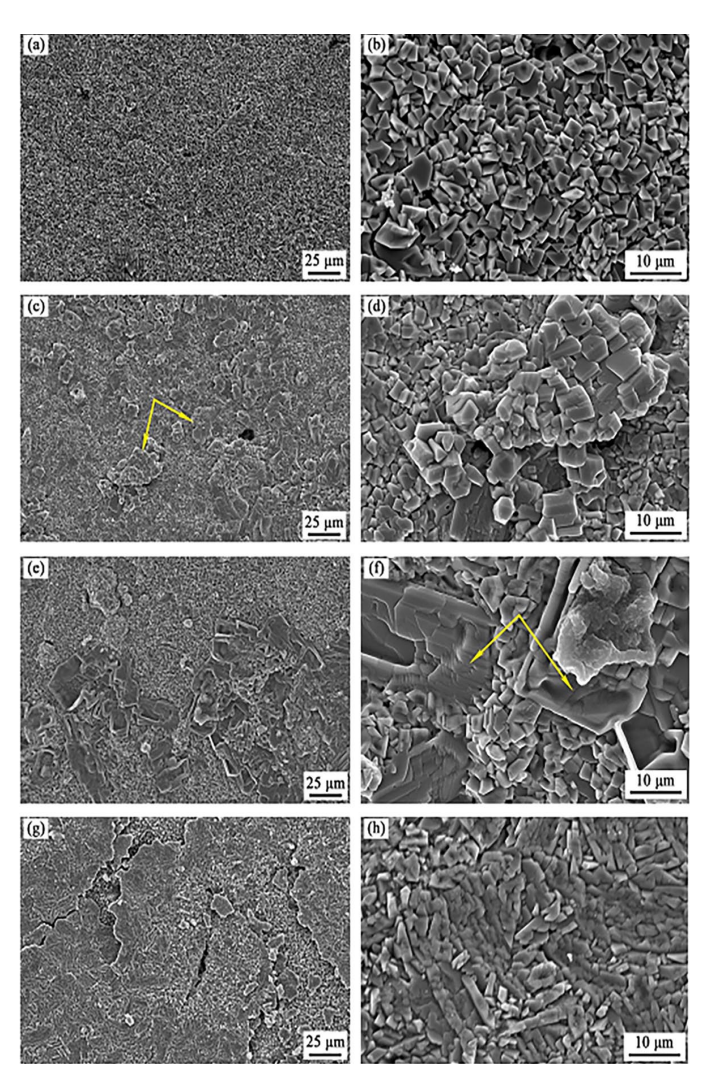


Fig. 3. Surface morphologies of Fe-V alloys after 180 min of oxidation at  $800^{\circ}\mathrm{C}$ 

## 3.4. Cross section morphologies of oxide layer

Fig. 4 presents a cross-sectional view of the oxide layer of Fe-V alloys after 180 minutes oxidation at 800°C, with yellow numbers denoting the thickness of the oxide layer. Obviously, the higher is the V content of the alloy, the thicker is the oxide layers. The average thickness of the oxide product layers for the Fe-7V, Fe-8V, Fe-9V, and Fe-11V alloys is approximately 31.177  $\mu$ m,

53.683 μm, 69.206 μm, and 92.891 μm, respectively, which is consistent with the overall weight gain order of the four samples depicted in Fig. 1. Furthermore, the oxide layers of the four Fe-V alloy samples display a loose and porous structure. As the V content increases, this characteristic becomes increasingly prominent, particularly in the middle position of the oxide layer (Fig. 4(d)), with a corresponding increase in both the number and size of pores. There are two main reasons for the loose tissue. Firstly, the Fe in the matrix undergoes an oxidation reaction. On the basis of the Fe-O phase diagram, when the oxidation temperature exceeds 570°C, the oxide layer transitions from Fe<sub>2</sub>O<sub>3</sub> on the outside to Fe<sub>3</sub>O<sub>4</sub> and FeO on the inside [19-21], where Fe<sub>3</sub>O<sub>4</sub> is a porous structure [22]. Secondly, alloy element V produces a low melting point of V<sub>2</sub>O<sub>5</sub> under high-temperature, which diffuses and evaporates within the oxide layer, leading to the formation of numerous pores in the oxide layer [23-24]. The porous structure of the oxide layer facilitates the entry of oxygen ions into the metal/oxide interface, serving as the primary reason for the sustained weight gain of Fe-V alloys under high-temperature oxidation conditions.

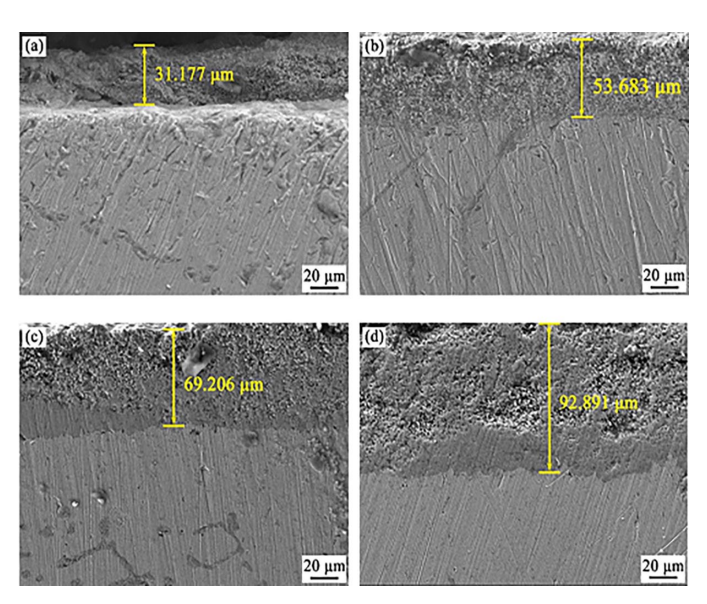


Fig. 4. The oxide layer cross-sectional of Fe-V alloys after 180 min oxidation at  $800^{\circ}$ C

Objective to further understand the composition of the oxide layer, the element distribution of the oxide layer cross-section of Fe-11V alloy was investigated by EDS analysis. As shown in Fig. 5, the enrichment of two main elements, Fe and O, in the oxide layer indicates that the primary component of the oxide layer is iron oxide. The V content is relatively low in the oxide layer and matrix, with no significant difference. This is attributed to the high affinity between V and O, leading to an early reaction with O in the initial stage of oxidation. As the oxidation progresses, a substantial portion is oxidized to  $V_2O_5$  and escapes from the matrix. There is also a small amount of vanadium oxide combined with  $Cr_2O_3$  to form a composite oxide of V and Cr (Fig. 2). Furthermore, as indicated in the line scanning, there is a sudden increase in the V content at certain positions, indicating

that these locations may have been VC regions before oxidation. During the oxidation process, the C element undergoes oxidation firstly, producing gas escape, which partially alleviates the oxidation of V in this region. The content of the Cr element does not exhibit significant differences between the oxide layer and matrix, suggesting that Cr undergoes an oxidation reaction in the oxide layer but fails to form a continuous and protective oxide film. This is consistent with the previous analysis results.

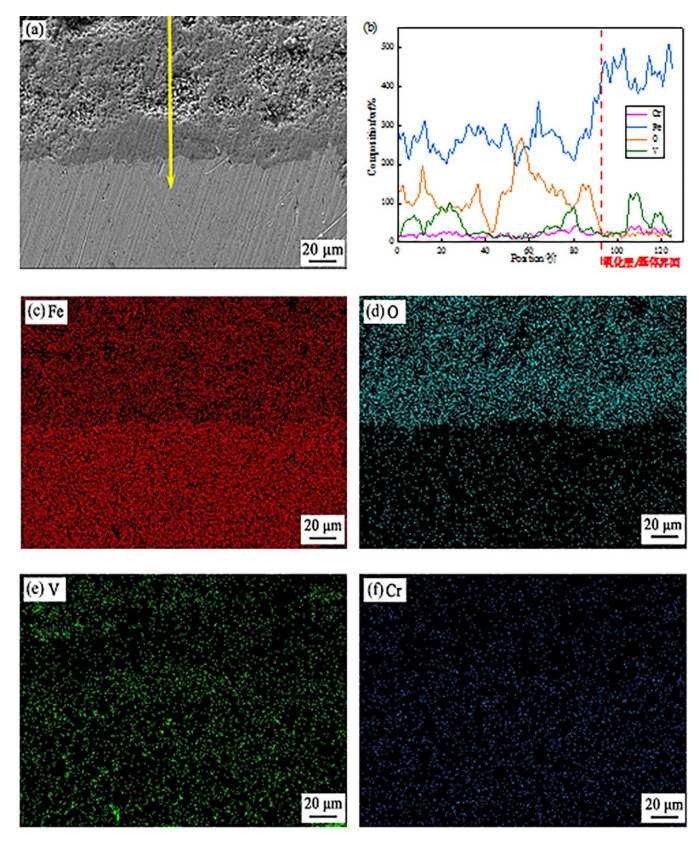


Fig. 5. The EDS spectra analysis of oxide layer cross-sectional of Fe-11V sample after oxidation for 180 min at 800°C

## 4. Conclusion

This study investigated the influence of different V contents on the high-temperature oxidation resistance of the Fe-V alloy at 800°C. XRD and FE-SEM/EDS techniques were conducted to observe and analyze the composition and morphologies of the oxide layer. The main conclusions can be drawn as follows:

- (1) The oxidation kinetics curves of Fe-V alloys at 800°C all follow a linear pattern. As the V content in the alloy increases, there is a corresponding increase in the weight gain per unit area of oxidation and a deeper degree of oxidation. After 180 minutes of oxidation, the Fe-11V sample exhibited a maximum weight increase of approximately 100.393 μg/mm² per unit area.
- (2) The oxide layer phase composition of the four Fe-V alloys includes Fe<sub>2</sub>O<sub>3</sub>, (Fe<sub>0.6</sub>Cr<sub>0.4</sub>)<sub>2</sub>O<sub>3</sub>, and CrVO<sub>4</sub>. None of these oxidation products possess antioxidant properties, thus incapable of inhibiting the oxidation of the alloy matrix.

- The oxidation process is determined by the reaction rate of generating oxides.
- (3) The formed oxide layer exhibits a loose and porous characteristic. With an increase in V content, the oxide layer thickens progressively, accompanied by a gradual rise in the number and size of pores within the oxide layer. The average thickness of the oxide layer in the Fe-7V, Fe-8V, Fe-9V, and Fe-11V alloys is approximately 31.177 μm, 53.683 μm, 69.206 μm, and 92.891 μm, respectively.

### Acknowledgements

This work was financially supported by Natural Science Foundation of Henan province [grant number 222300420437].

#### REFERENCE

- [1] J. Zhang, W. Zhang, Z. Xue, Oxidation Kinetics of Vanadium Slag Roasting in the Presence of Calcium Oxide. Min. Proc. Ext. Met. Rev. **38** (5), 265-273 (2017).
  - DOI: https://doi.org/10.1080/08827508.2017.1289197
- [2] G. Florian, K. von Klinski-Wetzel, J.N. Wagner, M Heilmaier, Influence of Vanadium on the Oxidation Resistance of the Intermetallic Phase Nb<sub>5</sub>Si<sub>3</sub>, Oxid. Met. 83, 119-132 (2015). DOI: https://doi.org/10.1007/s11085-014-9510-7
- [3] H. Wang, L. Teng, J. Zhang, S. Seetharaman, Oxidation of Fe-V Melts Under CO2-O2 Gas Mixtures. Metall. Mater. Trans. B 41 (5), 1042-1051 (2010).
   DOI: https://doi.org/10.1007/s11663-010-9391-3
- [4] R.K. Sharma, M. Singh, P. Kumar, G.B. Reddy, Oxidation of vanadium metal in oxygen plasma and their characterizations. AIP. ADV. 5, 887-898 (2015).
- [5] P. Chen, Z. Liu, R. Li, X. Li, The effect of manganese additions on the high temperature oxidation behaviour of the high-vanadium cast iron. J. Alloys Compd. 767, 181-187 (2018). DOI: https://doi.org/10.1016/j.jallcom.2018.07.113
- [6] U. Jain, J.Sonber, R.Tewari, High temperature oxidation behaviour of V-Ti-Ta alloys. Fusion. Eng. Des. 144,125-132 (2019). DOI: https://doi.org/10.1016/j.fusengdes.2019.04.070
- [7] N.A. Shaburova, A.O. Moghaddam, S.N. Veselkov, M.V. Sudarikov, O.V. Samoilova, E.A. Trofimov, High-Temperature Oxidation Behavior of AlxCoCrFeNiM (M = Cu, Ti, V) High-Entropy Alloys. Phys. Mesomech. 24, 653-662 (2021).
  DOI: https://doi.org/10.1134/S1029959921060035
- [8] K. Kusumoto, K. Shimizu, X. Yaer, H. Hara, K. Tamura, H. Kawai, High erosion-oxidation performance of Fe-based Nb or V containing multi-component alloys with Co addition at 1173 K. Mater. Des. 88, 366-374 (2015).
  - DOI: https://doi.org/10.1016/j.matdes.2015.08.161
- [9] B.F.O. Costa, G. Le. Caër, B. Malaman. Evolution of a Fe V sigma phase ball-milled in a mixture of argon and air. Hyperfine Interact **183** (1-3), 67-73 (2008).
  - DOI: https://doi.org/10.1007/s10751-008-9760-3

- [10] E. Dong, W. Yu, Q. Cai, L. Cheng, J. Shi, High-Temperature Oxidation Kinetics and Behavior of Ti–6Al–4V Alloy. Oxid. Met. 88, 719-732 (2017).
  - DOI: https://doi.org/10.1007/s11085-017-9770-0
- [11] Q. Li, S. Gu, L. Yu, F. Han, J. Dong, Separation of vanadium and chromium from vanadium-chromium slag by high-temperature heating. Sep. Purif. Technol. 336, 126098 (2024). DOI: https://doi.org/10.1016/j.seppur.2023.126098
- [12] B.F.O. Costa, G.L. Car, B. Malaman, Evolution of a FeV sigma phase ball-milled in a mixture of argon and air. Hyperfine Interact 183, 67-73 (2008). DOI: https://doi.org/10.1007/s10751-008-9760-3
- [13] J. Lu, Z. Yang, SQ. Xu, H. Zhao, Y. Gu, Oxidation behaviors of inconel 740H in air and dynamic steam. High Temperature Materials & Processes 35, 697-704 (2016). DOI: https://doi.org/10.1515/htmp-2014-0242
- [14] W. Wang, W. Wang, Q. Sun, Utilization of vanadium slag and ironrich red mud for the fabrication of Fe–V alloy: mechanism and performance analysis. J. Sustain. Metall. 9 (1), 341-349 (2023). DOI: https://doi.org/10.1007/s40831-023-00657-6
- [15] A.N. Tyumentsev, A.D. Korotaev, Y.P. Pinzhin, S.V. Ovchinnikov, V.M. Chernov, I.A. Ditenberga, A.K. Shikov, M.M. Potapenko, V.M. Chernov, Effect of internal oxidation on the microstructure and mechanical properties of vanadium alloys. J. Nucl. Mater. 367-370, 853-857 (2007).
  - DOI: https://doi.org/10.1016/j.jnucmat.2007.03.070
- [16] Y. Yin, Q. Tan, Y. Zhao, Q. Sun, M. Zhang, A Cost-effective Fe-rich compositionally complicated alloy with superior High-temperature oxidation resistance. Corros. Sci. 180, 109190 (2020). DOI: https://doi.org/10.1016/j.corsci.2020.109190

- [17] S. Zhang, L. Jia, Y. Guo, High-temperature oxidation behavior of Nb-Si-based alloy with separate vanadium, tantalum, tungsten and zirconium addition [J]. Rare Met. 40 (3), 607-615(2021). DOI: https://doi.org/10.1007/s12598-017-0916-7
- [18] M.H. Jeong, D.H. Lee, J.W. Bae, Reduction and oxidation kinetics of different phases of iron oxides. Int. J. Hydrogen. Energ. 40, 2613-2620 (2015).
- DOI: https://doi.org/10.1016/j.ijhydene.2014.12.099
  [19] M. Lin, C. Wang, A.A. Volinsky. High temperature oxidation
- [19] M. Lin, C. Wang, A.A. Volinsky. High temperature oxidation behavior of flake and spheroidal graphite cast irons. Oxid. Met. 76 (3-4), 161-168 (2011). DOI: https://doi.org/10.1007/s11085-011-9244-8
- [20] Y. Ustinovshikov, B. Pushkarev, I. Sapegina, Phase transformations in alloys of the Fe–V system. J. Alloys Compd. 398, 133-138 (2005). DOI: https://doi.org/10.1016/j.jallcom. 2005.02.030
- [21] J. Park, J.H. Shim, Y.K. Lee, Room-temperature solid solution softening in Fe–V binary system. Met. Mater. Int. 22 (1), 7-11 (2016).
  - DOI: https://doi.org/10.1007/s12540-015-5114-2
- [22] R.Y. Chen, W.Y.D. Yeun, Review of the high-temperature oxidation of iron and carbon steels in air or oxygen. Oxid. Met. **59** (5), 433-468 (2003).
- [23] K.H. Choe, S.M. Lee, K.W. Lee, High temperature oxidation behavior of Si-Mo ferritic ductile cast iron. Mater. Sci. Forum **654-656**, 542-545 (2010).
  - DOI: https://doi.org/10.4028/www.scientific.net/MSF.654-656.542
- [24] L. Ye, X. Xian, Y. Yang. Study on High-Temperature Oxidation Characteristics of Pure Vanadium. Adv. Mate. Res. **189-193**, 169-172 (2011).
  - DOI: https://doi.org/10.4028/www.scientific.net/amr.189-193.169